Int j simul model 24 (2025) 4, 635-646
Original scientific paper

SIMULATION OF PROPELLER AIRWORTHINESS FOR LOW-ALTITUDE AIRCRAFT

Si, Q. M.[*,**,#]; Hao, Z. H.[*]; Zhang, H.[*]; Qian, J. D.[***,****] & Guo, Y. Y.[*,**]
[*] School of Civil Aviation, Zhengzhou University of Aeronautics, Zhengzhou 450046, China
[**] Henan Key Laboratory of General Aviation Technologies, Zhengzhou 450046, China
[***] Flight Technology and Flight Safety Research Base of the Civil Aviation Administration of China, Civil Aviation Flight University of China, Guanghan 618307, China
[****] Luoyang Beijiao Airport CO., LTD, Luoyang 471001, China
E-Mail: siqingmin@zua.edu.cn ([#] Corresponding author)

Abstract
To address the incompatibility between the aircraft body and the propeller due to configuration changes during low-altitude aircraft upgrade, an investigation was conducted using the NACA 2414 airfoil as a case study. On the basis of flight requirements, the propeller geometry was designed using Profili software, and a three-dimensional model was constructed in SolidWorks through a layer-by-layer lofting method. Ansys software was employed to simulate and analyse the variations in lift, noise, deformation, and fatigue life of the propeller under aerodynamic performance conditions, revealing the power output, noise generation, and safe operational cycle of a carbon fibre propeller under different rotational intensities. Results indicate that, the constructed propeller can generate a lift force of 403.77 N at a rotational speed of 3000 RPM, meeting the safety requirements for the aircraft's maximum take-off weight (255.4 kg). In addition, at this rotational speed, the noise level is approximately 70 dB, and the maximum deformation is only 0.366 mm. When the rotational speed is adjusted to 1×10^5 RPM, the propeller blades can operate safely for 34.7 h before failure occurs.
(Received in August 2025, accepted in October 2025. This paper was with the authors 3 weeks for 1 revision.)

Key Words: Low-Altitude Aircraft, Propeller Design, Aerodynamic Characteristic Analysis, Finite Element Analysis

1. INTRODUCTION

With the continuous advancement of global urbanization and sustained population growth, urban ground transportation has gradually reached saturation. Existing transportation modes are approaching their carrying limits, with urban roads, subways, and light rail systems in major cities generally operating under overload conditions. This issue severely restricts the operational efficiency of urban transportation and affects the daily mobility of residents. For addressing this challenge, the promotion of urban air mobility and electric vertical take-off and landing (eVTOL) aircraft has become a key trend in global transportation transformation [1]. Unlike traditional fixed-wing aircraft, which generate lift through aerodynamic surfaces, most low-altitude aircraft – especially VTOL aircraft – rely directly on propeller systems driven by electric motors for lift, thrust, and attitude control [2, 3]. This unique propulsion method makes the performance of propellers not only a supplementary component for propulsion but also the core determinant of the aircraft's hover efficiency, endurance, payload capacity, vibration noise levels, and manoeuvring stability [4].

However, low-altitude aircraft often operate in complex aerodynamic environments influenced by ground effects, dense obstacles, and unsteady airflow generated by urban building clusters. Strict noise control requirements further complicate the design.

Designing low-altitude aircraft requires engineers to carefully balance multiple objectives, such as high lift during hover, stability and control during the transition phase, low drag and high efficiency during cruising, and low noise levels. Currently, there is no "universal" airfoil that can be applied to all low-altitude aircraft. There is also no consensus on the optimal configuration of the aircraft body, leading to various structural forms on the market, such as multirotors, tilt-wing, hybrid wings, and self-tilting designs [5]. Additionally, during product iterations of the same low-altitude aircraft, the structural design often differs from the initial version, making it difficult to generalize the best propeller configuration for a specific aircraft model. Thus, selecting airfoils with corresponding advantages based on specific design requirements and establishing suitable propeller configurations for simulation validation have become an urgent need for low-altitude aircraft manufacturers. In this context, conducting feasibility studies on customized airfoil propellers holds significant practical importance.

The remaining sections of this study are organized as follows: Section 2 provides a literature review, summarizing relevant study on the structure and design of low-altitude aircraft propellers. Section 3 outlines the selection of airfoils, the 3D modelling of the selected propellers, the mesh generation. Section 4 presents the aerodynamic performance simulation results, including lift, noise, deformation, and fatigue life analyses for the designed propellers. In Section 5, the entire study is summarized, and relevant conclusions are drawn.

2. STATE OF THE ART

As the primary propulsion system for low-altitude aircraft, the propeller's performance directly determines the aircraft's flight time and efficiency [6]. To achieve this objective, numerous scholars have conducted extensive study on high-efficiency propeller design and aerodynamic performance calculations [7]. For example, Shi et al. [8] applied an unsteady turbulence model with dynamic mesh overlapping to study the aerodynamic interference between the forward propeller's wake and the rear propeller in counter-rotating propellers. Wang et al. [9] demonstrated through detailed simulation that barnacle fouling significantly compromises propeller hydrodynamic performance, primarily through induced flow separation and the destabilization of tip vortex structures. Wang et al. [10] have demonstrated the efficacy of variable-pitch propellers in maintaining high efficiency across a wide range of rotational speeds. Xiang et al. [11] proposed a high-efficiency propeller design method that, given flight speed, propeller speed, thrust, diameter, number of blades, and airfoil, could calculate the geometric characteristics of the maximum-efficiency propeller. Yilmaz and German [12] presented an optimization method considering the transition flight phase, optimizing a multirotor tilt-wing aircraft for nominal cruising, transition, and hovering conditions. Traub [13] introduced a simplified propeller analysis and design method, incorporating the effects of stall using vortex theory. Droandi et al. [14] studied the interaction between two adjacent UAV propellers' wakes during hover, discovering that the rotor thrust coefficient increased as the separation distance decreased, significantly amplifying thrust fluctuations. Wei et al. [15] addressed the issue of drone propeller noise by incorporating a serrated leading-edge design that mimics the wing morphology of owls. Shukla and Komerath [16] investigated the aerodynamic characteristics of a set of side-by-side rotors, finding that rotor efficiency decreased as the distance between rotors and Reynolds number decreased, leading to intensified wake interference. Stokkermans et al. [17] studied the interaction between side-by-side and front–back rotor layouts during hover, transition, and cruise conditions. Adkins and Liebeck [18] proposed a numerical method for designing maximum-efficiency propellers' chord lengths and pitch angles under specified operating conditions. Yu et al. [19] proposed a design method for propellers that achieves a balance between high efficiency, low noise, and robust aerodynamic performance. Veldhuis and Heyma [20] and Sinnige et al. [21] analysed the impact of propeller installation position and rotational direction on the wing's lift-to-drag ratio, finding that positioning the propeller near the symmetrical plane and closer to the wingtip and deviating vertically from the leading edge improved the lift-to-drag ratio. Rubin and Zhao [22] elucidated the transition mechanism of propellers from axial-dominant to wing-like behaviour, defining a critical angle (*AOAinv*), where the wing-equivalent thrust component begins to dominate. The study of the aerodynamic performance of annular propellers has also gained initial attention, with Xiang et al. [23] proposing an improved design method for electric aircraft propellers and conducting wind tunnel tests on scaled propellers, demonstrating that the method is suitable for electric aircraft propeller design. Numerous scholars have conducted substantial theoretical and experimental study on propeller dynamics, laying the foundation for propeller design and development for low-altitude aircraft.

In summary, current academic study on aircraft propellers, while achieving in-depth results in areas such as network modelling, deformation effects, and installation positions, remains somewhat isolated. These studies often lack alignment with engineering feasibility and airworthiness requirements. Additionally, because of the lack of precedent, government regulatory bodies tend to apply strict standards when implementing quality certifications. Most existing study focuses on the physical performance of propellers, often lacking simulations and verifications for airworthiness compliance, which limits their practical application value.

In light of the shortcomings of existing research, this study begins by examining airfoils that directly affect propeller performance. With a self-tilting wing eVTOL as the aircraft model, airfoils are selected for three-dimensional modelling. Subsequent simulation experiments determine whether the propeller design meets the flight requirements of the aircraft and its airworthiness standards. This study aims to provide a standardized reference for propeller design in the emerging field of low-altitude aircraft.

3. METHODOLOGY

3.1 Selection of aircraft airfoil and propeller model construction

Before the finite element analysis of the aerodynamic and power characteristics of the propeller, the finite element model of the propeller was first established. The propeller model selected in this study is based on a self-tilting wing eVTOL configuration, a type of low-altitude aircraft. This aircraft is a single-seat, ultralight eVTOL aircraft with a maximum range of approximately 65 km. The aircraft features an eight-set ducted propeller and tilting ducted fan design, with a carbon fibre structure weighing only 142 kg. NACA 2414 is a typical airfoil with a moderate to low camber, widely used in general aviation owing to its balanced performance and good stall characteristics. Given the selected eVTOL's parameters, such as a length of 4.08 m, a width of 4.1 m, and a maximum take-off weight of 255.4 kg, an airfoil with a 10 cm chord length was chosen. The modelling was carried out using SolidWorks software, as shown in Fig. 1. The propeller has a diameter of 100 cm.

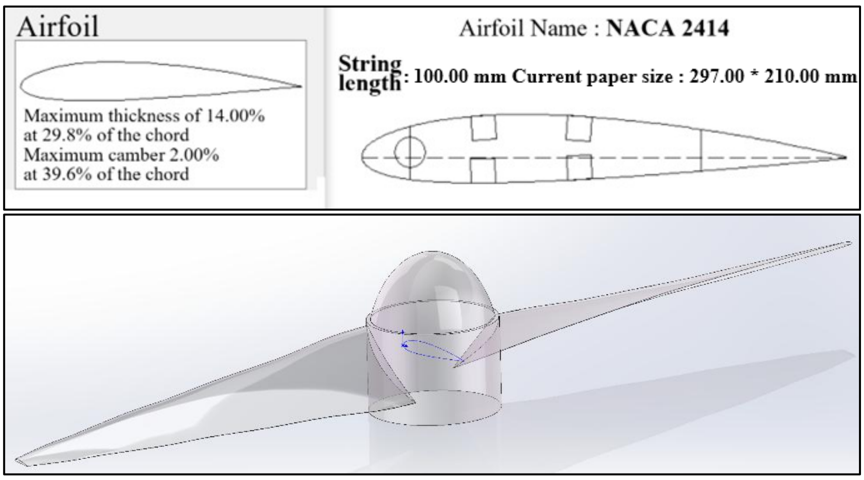

Figure 1: Finite element model of propeller.

3.2 Propeller computational domain and grid division

After the physical modelling of the propeller, the computational domain was divided on the basis of the modelled propeller. Taking the cavitation performance calculation of a ring-shaped propeller as an example, this study used the multiple reference frame method for calculation. The computational domain is illustrated in Fig. 2. It consists of three parts: The innermost layer includes the rotating domain of the ring-shaped propeller blade surface. The middle layer is the mesh refinement area of the enveloping rotating domain. This area is designed to improve the smoothness and reliability of the cavitation characteristic calculation, and it only affects the mesh division. The outer layer is the stationary domain, providing a surrounding air environment for the propeller's rotation. The stationary domain is set as a sphere, with all outlet surfaces established as pressure outlets to prevent external influences and allow for information exchange within the flow field caused only by internal propeller rotation. The characteristic length used is the propeller diameter, denoted as L. The rotating domain diameter is set to $1.2L$, the mesh refinement area diameter to $2.1L$, and the stationary domain radius to $5L$. For avoiding interference, the distance from the rotating domain to the boundary interface centre is set to $0.9L$, and the distance from the propeller blade surface to the upper surface of the rotating domain is set to $0.3L$.

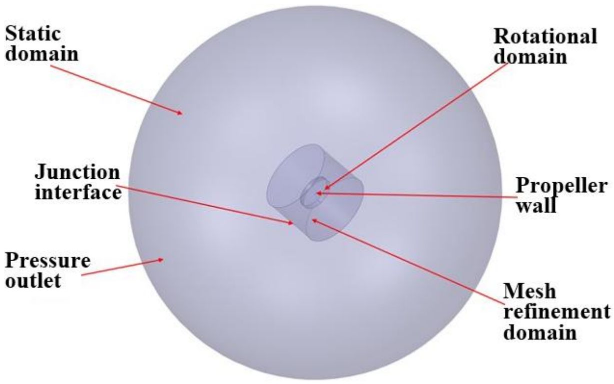

Figure 2: Division of computational domain for propeller.

The number and density of meshes directly affect the computational accuracy of computational fluid dynamics (CFD) software. Finer meshes have a stronger ability to capture flow field information but also reduce overall computational efficiency. To balance efficiency and accuracy, this study controlled the number of meshes by adjusting the minimum size of the propeller surface and the maximum size of the refinement area. The minimum mesh size for the rotating domain and mesh refinement area was set to 0.8 mm^3 to improve the accuracy of the simulation results, while the minimum mesh size for the stationary domain was set to 100 mm^3 to increase the mesh division speed. The results of the mesh division obtained under different methods are shown in Fig. 3.

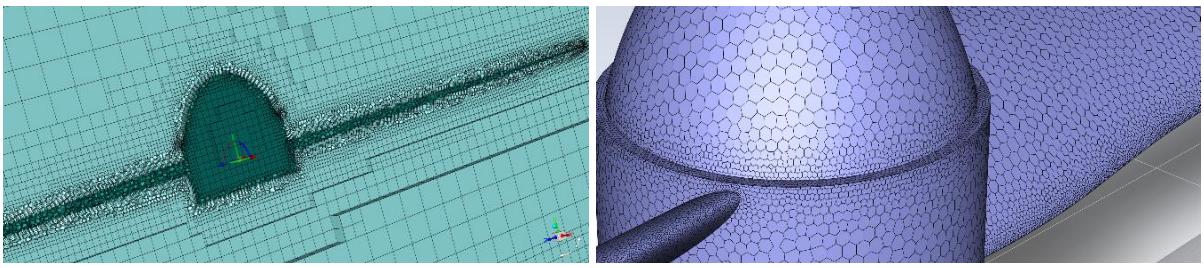

a) b)

Figure 3: Propeller body meshing and improvement; a) Propeller body grid generation, b) Improved surface mesh quality.

Mesh observation revealed that the generated number of mesh faces reaches millions, and the mesh division quality is good. In this experiment, the mesh quality was improved to 0.3 to enhance the accuracy of the subsequent simulation results.

4. ANALYSIS OF RESULTS

4.1 Simulation analysis of lift generated by the propeller

Combining predecessors' method of extracting the factors influencing aircraft runway excursion accidents, a total of 129 aircraft runway excursion accidents on a global scale during the period of 2010–2022 were collected and organized through the information reported by domestic and foreign mainstream media. On this basis, 20 experts dedicated to civil aviation safety management were interviewed through e-mail, phone call, and video conference to further optimally screen out influencing factors. By arranging and analysing the interview results, 21 simplified basic events leading to aircraft runway excursion events and their occurrence probability and 12 fault types were acquired according to the index division framework of man-machine-environment-management, as shown in Table I.

Table I: Carbon fibre material parameters.

Material properties	Size
Density	1600 kg/m^3
Coefficient of thermal expansion	$1.2 \cdot 10^{-5}$ °C^{-1}
Young's modulus	$2 \cdot 10^{11}$ Pa
Poisson's ratio	0.317
Bulk modulus	$1.82 \cdot 10^{11}$ Pa
Shear modulus	$7.6 \cdot 10^{10}$ Pa
Intensity coefficient	$2 \cdot 10^{9}$ Pa
Ductility coefficient	0.213
Cyclic strength coefficient	$1 \cdot 10^{9}$ Pa
Cyclic strain hardening exponent	0.2
Tensile yield strength	$2.5 \cdot 10^{8}$ Pa
Tensile yield strength	$4.6 \cdot 10^{8}$ Pa

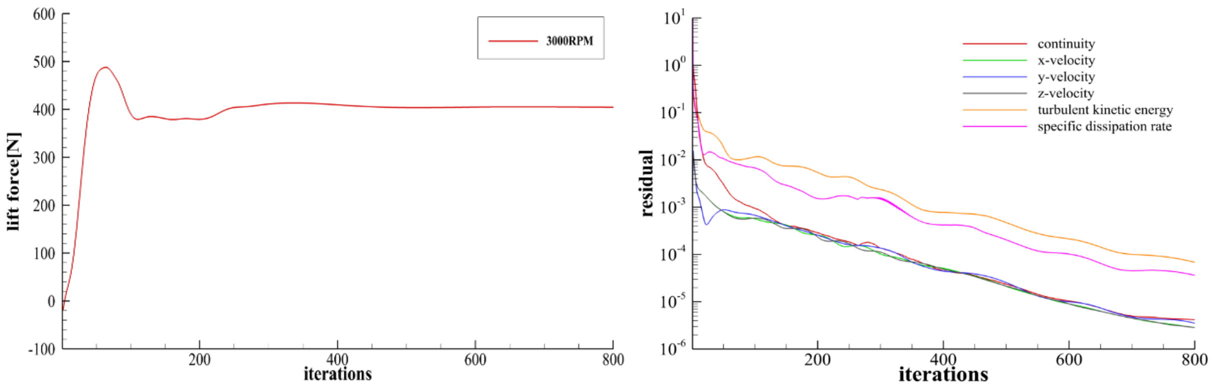

a) b)

Figure 4: Propeller lift and computational residuals; a) Magnitude of the generated lift, b) Residual variation during the process.

From Fig. 4, after 800 iterations, the simulation results stabilized, and the residual continuously decreased to the set value. Each propeller generated 403.77 N of lift at 3000 RPM. Given that the empty weight of the selected eVTOL model is 142 kg and the maximum take-off weight is 255.4 kg, with eight propellers providing lift, the simulated lift is sufficient to meet the actual operating weight of the selected low-altitude aircraft.

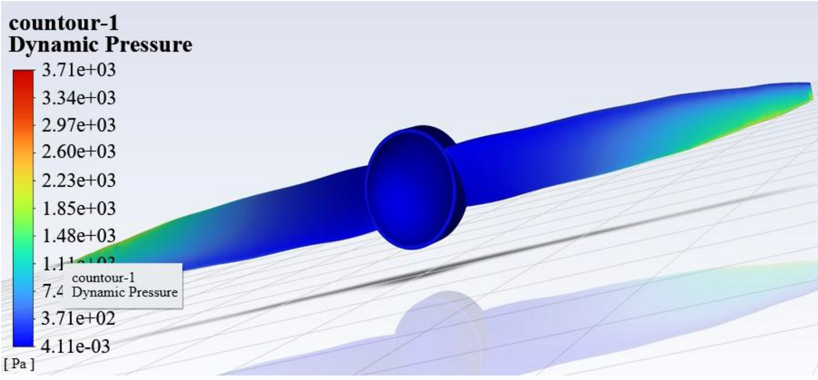

Figure 5: Lift generated by propeller.

Owing to the high tip speed of the propeller blades, the drag and friction at the edges are also high. Thus, the Newtonian force experienced by the propeller in Fig. 5 is accurate. Additionally, no issues, such as stall, stagnation, model deficiencies, or configuration errors, occurred during the propeller rotation simulation process. Hence, the propeller model established in this study meets the requirements for actual operation.

4.2 Simulation analysis of noise generated by the propeller

The operational characteristics of low-altitude vehicles, which frequently take off and land in low-altitude airspace, can directly radiate high-decibel noise in the range of 100–5000 Hz, with peak levels reaching 80–95 dB to surrounding communities. This noise pollution may intensify community resistance, hindering the implementation of airspace policies. Therefore, performing noise simulation on the modelled custom airfoil propeller to ensure it achieves an acceptable level is an essential step in determining whether the propeller model is qualified.

After the lift simulation of the propeller, noise simulation was conducted. The acoustic model in Fluent was activated, and the viscous model was changed to a large eddy simulation (LES) model. Compared with *k*-omega models, LES significantly enhances the accuracy of noise spectrum predictions, providing a reliable basis for noise reduction designs of rotating components such as propellers and airfoils. The propeller model was defined as the noise source, with eight measurement points uniformly distributed in a circle around the propeller to measure the noise levels. The specific setup is shown in Fig. 6.

Quantity 8

Receiver Name	X-coordinate (m)	Y-coordinate (m)	Z-coordinate (m)	File Name
receiver-1	-0. 65	0. 3	0	receiver-1
receiver-2	-0. 435	0. 3	0. 483	receiver-2
receiver-3	0	0. 3	0. 65	receiver-3
receiver-4	0. 5	0. 3	0. 416	receiver-4
receiver-5	0. 65	0. 3	0	receiver-5
receiver-6	0. 427	0. 3	-0. 49	receiver-6
receiver-7	0	0. 3	-0. 65	receiver-7
receiver-8	-0. 465	0. 3	-0. 454	receiver-8

Figure 6: Measurement position of propeller noise.

Because this experiment involved transient noise simulation, the number of time steps was set to 500, and the time step length was set to $2{\cdot}10^{-4}$ s to measure the noise levels within 0.1 s when the propeller reaches a constant 3000 RPM. The simulation ran until it stopped, and the residual variation curve is presented in Fig. 7.

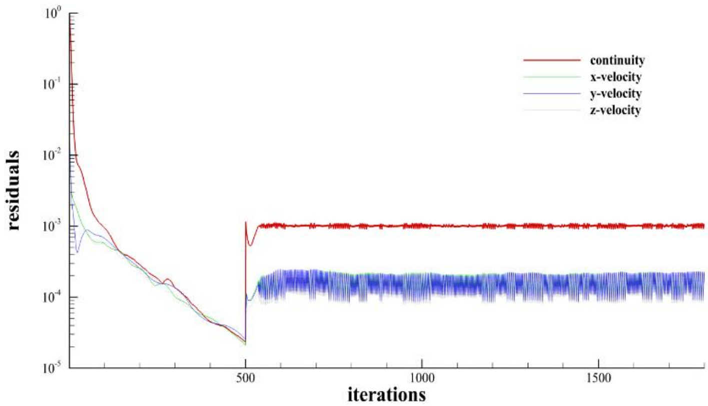

Figure 7: Residual change during propeller noise simulation.

During the first 500 iterations, the residual continuously decreased, and the measured changes in lift, drag, etc. showed a trend toward stability. After the 500th iteration, the transient noise simulation residual eventually fluctuated, indicating that the noise generated by the propeller changed continuously during this period, in line with the physical characteristics of noise fluctuations. The noise variation measured surrounding points is shown in Fig. 8.

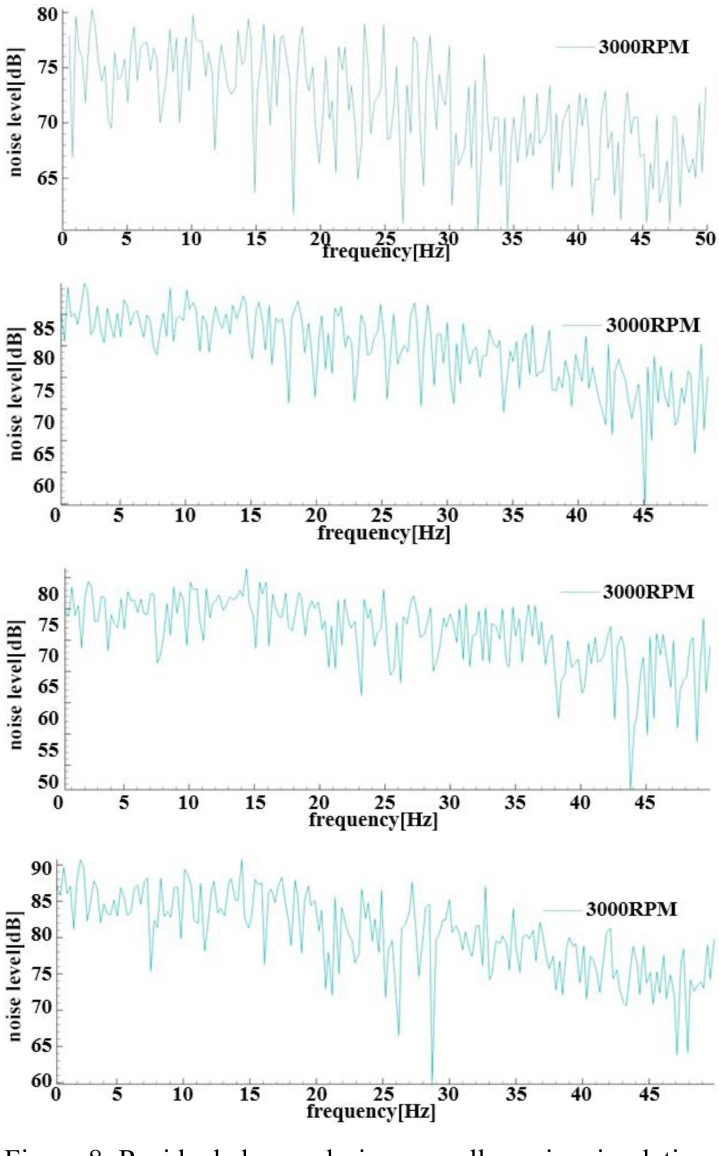

Figure 8: Residual change during propeller noise simulation.

By combining the noise measurements from the eight detection points and observing when the fluctuations stabilized at each point, this study found that each propeller generated an average noise level of approximately 60–80 dB at 3000 RPM. This simulation corresponds to the theoretical maximum speed of the propeller during the take-off phase. In practice, the noise generated by the vehicle was lower than the simulation results. Currently, no specific regulations exist for low-altitude vehicles. Hence, for certification purposes, the standards for propeller-driven small aircraft and propeller commuter aircraft are generally used. According to China's CCAR-36-R3, for single-engine aircraft that receive the initial type-certification application after April 15, 2007, when the maximum certified take-off weight is equal to or less than 570 kg, the noise level must not exceed 70 dB. For weights exceeding 570 kg, the noise limit increases logarithmically with the aircraft's weight; for every doubling of weight, the noise increases by 10.75 dB, up to a maximum of 85 dB, after which the noise level remains constant up to 8618 kg.

In conclusion, the selected eVTOL model's lift system consists of eight propellers, with a maximum take-off weight of 255.4 kg, which is below the 570 kg limit set by CCAR-36-R3. The total noise generated by all the propellers is less than the minimum required level of 70 dB. Therefore, the established propeller model meets the noise certification standards for propeller commuter aircraft.

4.3 Structural deformation simulation analysis of the propeller

Propeller design must not only meet enterprise requirements but also comply with relevant civil aviation regulations in China. In particular, Articles 35.35–35.39 of CCAR-35 specify that the detachable propeller hub and blade attachment devices must withstand centrifugal loads equal to twice the maximum centrifugal force generated by the propeller when operating within the prescribed limits. This test can be conducted either by a rotational test or a static tensile test. In addition, every primary load-bearing metal component must undergo fatigue evaluation and fatigue limit determination. Such fatigue evaluations must consider all reasonably foreseeable vibration load patterns, and the fatigue limit must also take into account the permissible service damage:

(1) A 10 h endurance bench test at the rated rotational speed using a propeller of the maximum pitch and diameter specified in the type certification.

(2) A 50 h flight test in level flight or climb, in which the propeller operates at rated speed for at least 5 h. During the remaining hours of the 50 h test, the propeller must operate at not less than 90 % of the rated speed. The propeller used must have the maximum diameter specified in the type certification.

(3) A 50 h endurance bench test at the certified power and propeller speed, using a propeller of the maximum diameter specified in the type certification.

In the Workbench environment, a static structural module was established. After the engineering materials were set in accordance with Table I, the physical model and mesh of the propeller generated in Fluent were imported. In the model setup, the material of the propeller was changed from the default structural steel to carbon fibre. Because the modelled propeller lacked the motor that supports its rotation, an additional cylindrical support was introduced at the central shaft of the propeller. A rotational speed of 3000 RPM was applied to this central shaft, and the static structural simulation was carried out. The resulting deformation is shown in Fig. 9.

When the propeller operates at high rotational speed, the region most susceptible to deformation is located at the trailing edge of the blades. Under the 3000 RPM condition, the deformation magnitude in this region was only 0.366, while other parts of the blade exhibited minimal deformation.

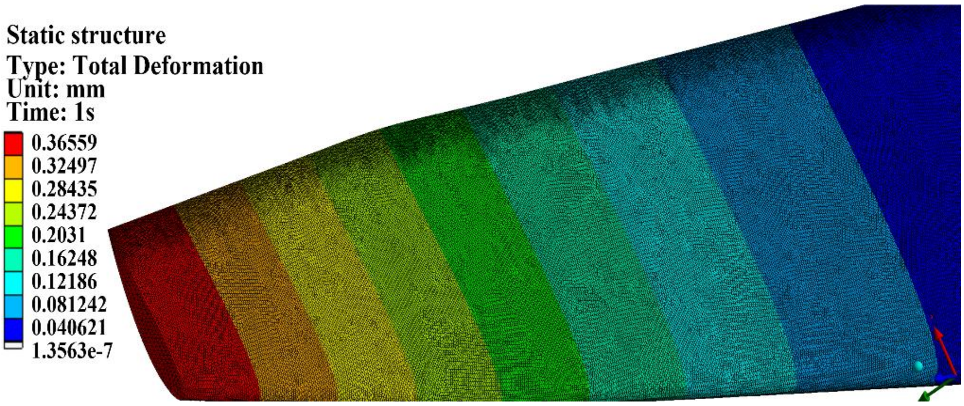

Figure 9: The structural deformation condition of the propeller during high-speed rotation.

The trailing edge corresponds to the region experiencing the largest centrifugal force during rotation, indicating that the test for blade attachment devices specified in Article 35.35 of CCAR-35 meets the Chinese civil aviation airworthiness standards. By adding the stress analysis tool and enabling the safety factor contour, as shown in Fig. 10, this study observed that except for a slightly lower safety factor at the junction between the blade and the propeller hub, most areas of the propeller maintained a safety factor around 15, representing a structurally safe condition. Therefore, the structural strength of the customized propeller model satisfies the requirements specified by the relevant airworthiness regulations.

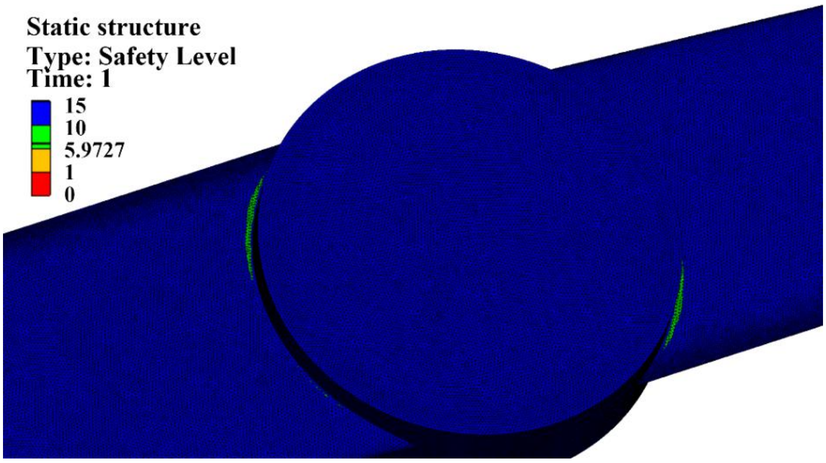

Figure 10: The safety factor of the propeller blade during high-speed rotation.

4.4 Fatigue life simulation analysis of the propeller

Simulation-based life prediction can optimize maintenance cycles, avoid excessive repairs that increase costs, and prevent downtime losses caused by unexpected failures. It is a key technological pillar supporting commercial-scale operations. Building upon the established high-speed rotation model of the propeller from the deformation study, further simulation study was conducted. Given that carbon fibre was used as the material for the propeller and considering its intrinsic material properties, the expected life of the propeller was set to $1 \cdot 10^6$ cycles. In the simulation setup, the fatigue toolbox was activated, with the transverse load set to a baseline of 0, and the average stress was configured as an equivalent stress. The proportional factor was set to 5 to clearly observe the changes in the fatigue sensitivity curve. Because, in actual operation, the propeller's lifespan is reduced owing to various resistances and friction, resulting in a shorter operational life compared with the simulated lifespan, the fatigue strength factor was set to 0.8 during the simulation to account for this difference. The resulting structural life and damage cloud plot are shown in Fig. 11.

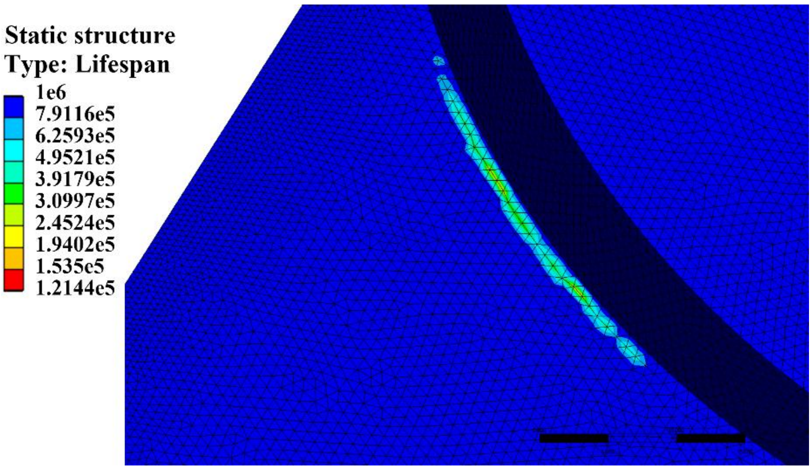

Figure 11: Structural life of propeller during high-speed rotation.

Based on the two images, the majority of the blade achieves the expected lifespan during high-speed rotation. Given that the simulation step was set to 1 s with a proportional factor of 5, this finding indicates that the modelled propeller can operate for 34.7 h at $1 \cdot 10^5$ RPM rotation speed before any blade or hub interface failure occurs. This result complies with Article 35.39 of CCAR-35, which specifies a 10 h endurance test for a propeller with a maximum pitch and fixed speed. After 277.7 h, the entire propeller eventually fails, fulfilling the requirement for 50 h of level flight rotation at 90 % of the rated speed. These results also comply with China's airworthiness standards for propellers. The minimum operational lifespan when the propeller fails under different proportional factors is shown in Fig. 12.

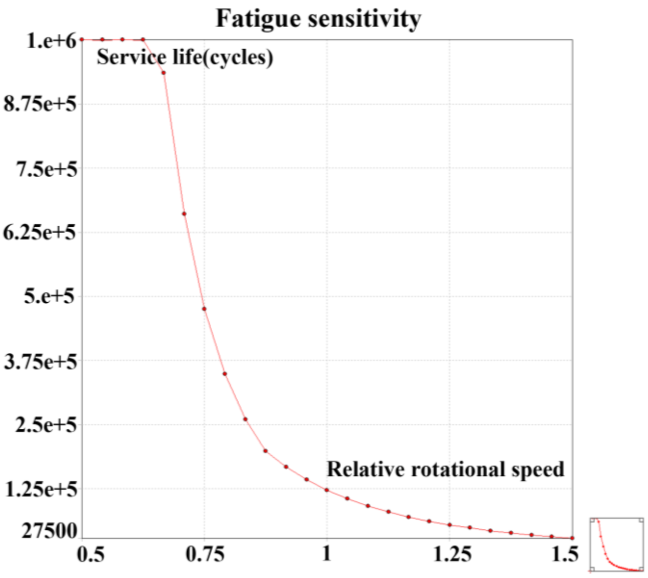

Figure 12: Fatigue sensitivity of propellers during high-speed rotation.

Because the highest operational speed of the modelled propeller is 3000 RPM, with an environmental intensity factor set to 0.2, Fig. 12 demonstrates that under actual operational conditions, the entire blade section of the propeller meets the expected lifespan cycle. Therefore, the established propeller passes the fatigue life test, confirming its compliance.

5. CONCLUSIONS

This study focuses on the propeller required for the self-tilting tilt-wing eVTOL configuration, utilizing SolidWorks software to model the propeller on the basis of the selected airfoil curvature and length. Ansys software was then used to perform aerodynamic and structural finite element analyses. The lift generated by the propeller blades during the take-off phase and the associated noise levels were simulated. The effects of blade deformation and failure time during high-speed rotation were also explored. The following conclusions were drawn:

(1) The carbon fibre propeller with a diameter of 1 m, constructed with NACA 2414 airfoil, produces 403.77 N of lift at the maximum take-off speed of 3000 RPM. This value is sufficient to meet the power requirements of the self-tilting tilt-wing eVTOL, which is composed of eight propellers and has a maximum take-off weight of 255.4 kg.

(2) During rotation at maximum take-off speed, the propeller generates approximately 70 dB of noise and exhibits a maximum deformation of 0.366, located at the blade tip. Under actual operating conditions, the propeller complies with the CCAR-36-R3 flight noise limitations and the propeller deformation requirements specified in Article 35.35 of CCAR-35.

(3) In a durability test in which the propeller rotates at 5 times the maximum take-off speed, the blades operate normally for 34.7 h before failure occurs. Full failure is observed after 277.7 h, satisfying the 50 h fatigue life requirement as per Article 35.39 of CCAR-35.

Although this study provides a valuable numerical simulation approach for propeller design in the field of low-altitude aircraft study, certain limitations exist, particularly in terms of airworthiness. For more stringent and precise airworthiness studies of propellers, software simulation and actual hardware testing are necessary. Future study will focus on the latest low-altitude aircraft airworthiness regulations and will conduct more rigorous and standardized airworthiness studies of propellers, taking into account more complex environmental factors such as strong wind interference and natural corrosion.

ACKNOWLEDGEMENT

This work was financially supported by the Key Research Projects of Higher Education Institutions in Henan Province (Grant No. 24A620005), Key Research and Development Program in Henan Province (Grant No. 241111242200), General Program of Natural Science Foundation of Henan Province (Grant No. 252300420070), Scientific Research Team Plan of Zhengzhou University of Aeronautics (Grant No. 24ZHTD02002), Youth Research Funds Plan of Zhengzhou University of Aeronautics (Grant No. 25ZHQN01007), Open Foundation of Henan Key Laboratory of General Aviation Technology (Grant No. ZHKF-250202), Graduate Education Innovation Program Fund of Zhengzhou University of Aeronautics (Grant No. 2025CX145).

REFERENCES

[1] Qin, B.; Wang, L. (2002). Review of unmanned aerial vehicle development, *Winged Missiles Journal*, Vol. 2002, No. 8, 4-10, doi:10.16338/j.issn.1009-1319.2002.08.004

[2] Guo, X. Y.; Zeng, Z.; Li, M. X.; Fu, S. (2022). Simulation of aircraft cabin evacuation strategy based on exit flow equilibrium, *International Journal of Simulation Modelling*, Vol. 21, No. 2, 261-272, doi:10.2507/IJSIMM21-2-601

[3] Fike, M.; Pezdevsek, M.; Predin, A.; Hren, G. (2023). Blade element momentum calculation method with various corrections, *International Journal of Simulation Modelling*, Vol. 22, No. 3, 404-415, doi:10.2507/IJSIMM22-3-647

[4] D'Angelo, S.; Berardi, F.; Minisci, E. (2002). Aerodynamic performances of propellers with parametric considerations on the optimal design, *The Aeronautical Journal*, Vol. 106, No. 1060, 313-320, doi:10.1017/S0001924000096068

[5] Han, Z. H.; Gao, Z. H.; Song, W. P.; Xia, L. (2021). On airfoil research and development:history, current status, and future directions, *Acta Aerodynamica Sinica*, Vol. 39, No. 6, 1-36, doi:10.7638/kqdlxxb-2021.0396

[6] Zeng, Z.; Lan, F. Y.; Wang, Y. S. (2024). A simulation method of site selection for liquid ammonia tanks, *International Journal of Simulation Modelling*, Vol. 23, No. 2, 287-298, doi:10.2507/IJSIMM23-2-685

[7] Liu, P.-Q.; Geng, X.; Hu, T.-X.; Ge, Y.-S.; Lyu, C.-H.; Liu, J.-J. (2023). Research progress on aerodynamics, noise and optimization design for modern aviation propellers, *Acta Aerodynamica Sinica*, Vol. 41, No. 10, 62-78, doi:10.7638/kqdlxxb-2023.0058
[8] Shi, W.-B.; Li, J.; Yang, Z.; Zhang, H. (2018). CFD analysis of contrarotating open rotor aerodynamic interactions, *International Journal of Aerospace Engineering*, Vol. 2018, Paper 9538787, 13 pages, doi:10.1155/2018/9538787
[9] Wang, Z.; Wu, T.; Wang, L.; Cao, W.; Luo, W. (2024). Near-field wake dynamics of propellers affected by double-sided barnacles attachment, *Physics of Fluids*, Vol. 36, No. 10, Paper 105177, doi:10.1063/5.0237079
[10] Wang, D.; Song, B.; Jiao, J.; Xue, D. (2023). High-altitude airship variable-pitch propeller performance analysis at multiple altitudes, *Proceedings of the Institution of Mechanical Engineers, Part G: Journal of Aerospace Engineering*, Vol. 237, No. 13, 2961-2973, doi:10.1177/09544100231167710
[11] Xiang, S.; Wang, J.; Zhang, L.-G.; Tong, S.-X.; Wu, J.; Liu, Y.-Q. (2015). A design method for high efficiency propeller, *Journal of Aerospace Power*, Vol. 30, No. 1, 136-141, doi:10.13224/j.cnki.jasp.2015.01.019
[12] Yilmaz, E.; German, B. J. (2024). Control allocation optimization for an over-actuated tandem tiltwing eVTOL aircraft considering aerodynamic interactions, *Aerospace Science and Technology*, Vol. 155, Part 1, Paper 109595, 23 pages, doi:10.1016/j.ast.2024.109595
[13] Traub, L. W. (2016). Simplified propeller analysis and design including effects of stall, *The Aeronautical Journal*, Vol. 120, No. 1227, 796-818, doi:10.1017/aer.2016.31
[14] Droandi, G.; Zanotti, A.; Gibertini, G.; Grassi, D.; Campanardi, G. (2015). Experimental investigation of the rotor-wing aerodynamic interaction in a tiltwing aircraft in hover, *The Aeronautical Journal*, Vol. 119, No. 1215, 591-612, doi:10.1017/S0001924000010708
[15] Wei, Y.; Xu, F.; Bian, S.; Kong, D. (2020). Noise reduction of UAV using biomimetic propellers with varied morphologies leading-edge serration, *Journal of Bionic Engineering*, Vol. 17, No. 4, 767-779, doi:10.1007/s42235-020-0054-z
[16] Shukla, D.; Komerath, N. (2018). Multirotor drone aerodynamic interaction investigation, *Drones*, Vol. 2, No. 4, Paper 43, 13 pages, doi:10.3390/drones2040043
[17] Stokkermans, T. C. A.; Usai, D.; Sinnige, T.; Veldhuis, L. L. M. (2021). Aerodynamic interaction effects between propellers in typical eVTOL vehicle configurations, *Journal of Aircraft*, Vol. 58, No. 4, 815-833, doi:10.2514/1.C035814
[18] Adkins, C. N.; Liebeck, R. H. (1994). Design of optimum propellers, *Journal of Propulsion and Power*, Vol. 10, No. 5, 676-682, doi:10.2514/3.23779
[19] Yu, P.; Peng, J.; Bai, J.; Han, X.; Song. X. (2020). Aeroacoustic and aerodynamic optimization of propeller blades, *Chinese Journal of Aeronautics*, Vol. 33, No. 3, 826-839, doi:10.1016/j.cja.2019.11.005
[20] Veldhuis, L. L. M.; Heyma, P. M. (2000). Aerodynamic optimization of wings in multi-engined tractor propeller arrangements, *Aircraft Design*, Vol. 3, No. 3, 129-149, doi:10.1016/S1369-8869(00)00010-0
[21] Sinnige, T.; de Vries, R.; Della Corte, B.; Avallone, F.; Ragni, D.; Eitelberg, G.; Veldjuis, L. L. M. (2018). Unsteady pylon loading caused by propeller-slipstream impingement for tip-mounted propellers, *Journal of Aircraft*, Vol. 55, No. 4, 1605-1618, doi:10.2514/1.C034696
[22] Rubin, R. L.; Zhao, D. (2022). Identifying the propeller transition to wing-like behavior at high angles of incidence, *AIAA Journal*, Vol. 60, No. 4, 2308-2323, doi:10.2514/1.J060932
[23] Xiang, S.; Liu, Y. Q.; Tong, G.; Zhao, W.-P.; Tong, S.-X.; Li, Y.-D. (2018). An improved propeller design method for the electric aircraft, *Aerospace Science and Technology*, Vol. 78, 488-493, doi:10.1016/j.ast.2018.05.008